Brodogradnja Volume 77 Number 1 (2026) 77105

journal homepage: www.brodogradnja.fsb.hr

Brodogradnja

An International Journal of Naval Architecture and Ocean Engineering for Research and Development

# Numerical investigation of the hydrodynamic characteristics and interactions of an unmanned surface vehicle chasing a mother ship during recovery

*Gong Xiang[1,2,3], Kunpeng Rao[1], Haotian Wang[1], Xianbo Xiang[1,2,3], Mingjiu Zuo[4*], Shan Wang[5], Carlos Guedes Soares[5]*

[1] *School of Naval Architecture and Ocean Engineering, Huazhong University of Science and Technology, 1037 Luoyu Road, Wuhan, China*
[2] *International Science and Techmology Cooperation Offshore Center for Ship and Marine Intelligent Equipment and Technology, 1037 Luoyu Road, Wuhan, China*
[3] *Wuhan Belt & Road Joint Lab of Ship and Marine Intelligent Equipment and Technology, 1037 Luoyu Road, Wuhan, China*
[4] *College of Electronic Engineering, Naval University of Engineering, Wuhan 430032, China*
[5] *Centre for Marine Technology and Ocean Engineering (CENTEC), Instituto Superior Tecnico, Universidade de Lisboa, Lisbon, Portugal*

**ARTICLE INFO**

Keywords:
Unmanned surface vehicle
Hydrodynamic interaction
CFD
Motion responses and loads
Chasing mother ship

**ABSTRACT**

Unmanned surface vehicles (USVs) require efficient and reliable recovery at sea. However, the recovery process, involving USVs chasing a mother ship, is complex and risky due to wave-making and wake effects that impact USV stability and resistance. It is necessary to study the interaction between the USV and the mother ship during the docking process in order to understand the changes in the motion performance of the unmanned ship during docking and provide a basis for the subsequent optimization of the control method and recovery path of docking recovery. This study numerically simulates the hydrodynamic behaviors of a 175-USV developed by Huazhong University of Science and Technology chasing alongside a KRISO Container Ship (KCS) standard model during recovery. 175-USV lake tests and corresponding simulations were compared and analyzed, which show good accuracy. Simulations reveal time-varying hydrodynamic characteristics as the USV operates into calm water, in coming waves of varying amplitudes and directions. Findings show roll angles and moments fluctuate within the location range of 35-45 % of the mother ship length to the stern, with swaying force peaking near the location of 10 % of mother ship length to the stern due to suction effects. Waves increase motion responses and loads, especially under oblique wave conditions, yet smoother regions persist on the opposite side of incoming waves. This study reveals the interaction between the hydrodynamic properties and the ship during docking, which supports the safe and reliable recovery of unmanned vessels.

## 1. Introduction

With the development of unmanned technology, USV play an important role in many fields such as patrol, search and rescue, maritime confrontation [1]. USVs need to complete the recovery by chasing the mother

* Corresponding author
E-mail address: zuomingjiu@126.com

https://doi.org/10.21278/brod77105
Received 21 April 2025; Received in revised form 14 July 2025; Accepted 4 August 2025
Available online 12 September 2025
ISSN 0007-215X; eISSN 1845-5859

ship autonomously, also called docking in many missions, to extend the endurance range or prepare for the next mission. Currently, unmanned surface vehicles are mainly recovered in two ways: from the side of the mother ship and from the stern (corresponding to two docking recovery paths, approaching from the rear of the mother ship and approaching from the side of the mother ship, respectively). As shown in Figure 1, there are three common methods of launching and recovering USVs: 1. hoisting; 2. stern slide; and 3. docking. The second method performs better in terms of equipment space requirements, launch and recovery time, and sea condition restrictions. Among them, the hydrodynamic characteristics of the USV during docking and recovery are one of the key factors affecting its success rate and safety. In the docking process, the USV needs to maintain a stable attitude and trajectory under complex sea conditions such as currents and waves, which puts forward strict requirements on its hydrodynamic performance [2-4]. During the docking process, the interaction between the USV and the mother ship will lead to significant changes in the USV encountered environment, like sea currents, waves, etc, thus reducing the manoeuvring performance and docking accuracy of the USV.

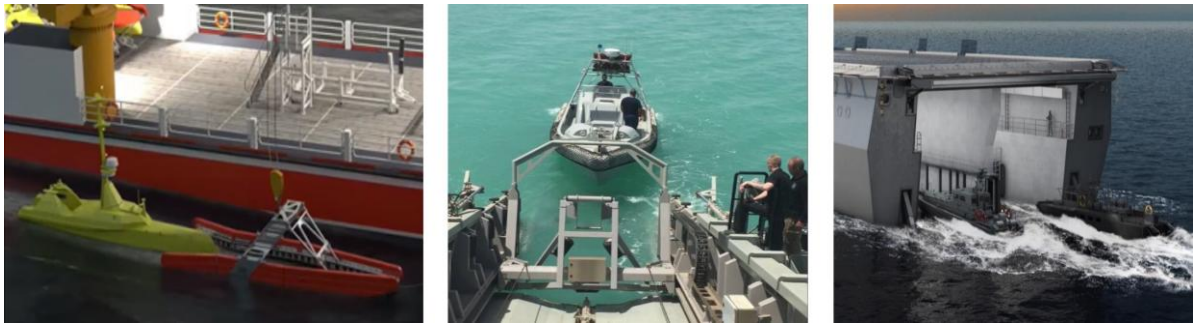

**Fig. 1** USV recovery process, left: Lifting type, Middle: Stern Sliding type, right: Docking Bay type

Hydrodynamic characteristics of USV mainly include hydrodynamic forces, wave loads, buoyancy changes and dynamic responses of the target. The challenges faced in docking process of the USV include changes in hydrodynamic coefficients, such as significant changes in the USV's hydrodynamic coefficients (e.g., drag and lift) during low-speed navigation near the coast [5-7], leading to increased uncertainty in mathematical models. other challenges include environmental disturbances [8], nonlinear characteristics of USV models [9], and shallow-water effects [10], including shore effects and depth limitations in shallow water areas, which further complicate hydrodynamic modeling. Additionally, hydrodynamic force and wave load will cause the USV to produce out of vertical plane motions such as rolling, and lateral movement [11], thus affecting the precision and stability of docking operation [12-14]. There are three common ways of USV stowage and retrieval: 1. lifting type; 2. stern sliding type; 3. docking bay type. Among them, the lifting type has a better overall performance in terms of space requirements and time consuming [12, 15]. In the process of docking and recovery of unmanned surface vehicle, the USV is greatly influenced by the wake and waves of the mother ship, which may produce motion response unfavourable to the recovery. Studying the motion interference of the mother ship on the USV is essentially a study of the hydrodynamic interactions between multiple floating bodies, and its research methods mainly include model tests, empirical formulas and numerical simulations. The model test requires a long test period and high-test cost, and the empirical formula requires several tests to formulate and is limited by the shape of the floating body. Numerical simulation methods can avoid these drawbacks and provide more data for the hydrodynamic interactions between ships. Classical numerical simulation methods are usually based on potential flow theory. Ohkusu [16] used two-dimensional slice theory to study the hydrodynamic effects of two cylindrical models during forced motion at the water surface. Yeung [17] applied slender-body theory to study the non-stationary hydrodynamic interactions of two ships moving in shallow water. Liu and Zou [18] used three-dimensional linear potential flow theory to calculations and verified the reliability of the calculation procedure by comparing it with experimental results. Chen and Wu [8] investigated the staggered motion of two vehicles in shallow water based on the G-N equations and analyzed the non-constant wave interference characteristics. Sutulo et al. [19] calculated the inter-vehicle hydrodynamic interactions using a procedure based on the classical Hess and Smith method, independent of the influence of hull shape and mutual position and motion of interacting bodies

and validated with experimental data. Nam and Park [20] proposed a time-domain numerical method based on a three-dimensional potential-flow solver to investigate the ship crossing effect and the hydrodynamic forces generated by its waves on a dock-moored barge. Li [21] used linear hydrodynamics based on potential-flow theory with the use of the Cummins time-domain equations to simulate the motion of the ship and discussed the hydrodynamic characteristics of the floating oil recovery vessel under parallel and non-parallel motion with the ship based on the gap resonance mode. Huang et al. [22] proposed a numerical method based on the Hess and Smith surface element method to calculate the intership hydrodynamics during parallel navigation and meeting of two ships, and compared with the experimental data, verified its accuracy in medium-shallow water and medium-low speed. Zheng [23] compared the effects of different docking methods on the motion patterns of the two vessels under different wave directions based on the linear potential flow theory. Tafazzoli et al. [24] carried out a coupled time-domain dynamics analysis based on the boundary element method to study the hydrodynamic effects between the FPSO and the shuttle oil tanker and considered the effects of the distance and the relative angle between the oil tanker and the FPSO on the dynamic response of the two vessels. Ma et al. [25] used the three-dimensional frequency domain potential flow theory to study the coupled motion of the two ships in waves, solved the velocity potential by means of boundary integral equations constructed by moving the pulsation source Green's function, and computed and analyzed the coupled motion of the two ships under different operating conditions. Cong et al. [26] used the boundary integral equation method and the higher-order boundary element method to solve the wave in positive and oblique waves and the wave along the long vertical wall of the interaction of the ship was calculated for linear free water surface height, wave loads and second-order mean wave drift loads.

In recent years, more and more researchers have analyzed the hydrodynamic interactions between ships through the computation of viscous flow. In 2009, Huang et al. [22] solved the mutual hydrodynamic forces between ships using the RANS method and investigated the hydrodynamic interferences between the two ships in the absence of relative motion. Zhang [8] used Fluent to solve the RANS equations to simulate the parallel straight-line sailing of two ships in shallow water, and analyzed the effects of factors such as pairwise spacing, ship scale ratio and speed on the inter-ship hydrodynamics. Zou and Larsson [27] used the steady-state Reynolds-averaged Navier-Stokes solver to study the inter-ship interactions. The effects of water depth, speed, transverse and longitudinal distances between two ships on inter-ship hydrodynamics were analyzed. Liu and Zou [18] applied CFD software to discuss the rendezvous problem of two ships in shallow and narrow waters, calculated their interacting hydrodynamics, and simulated a variety of ship types under different water depths, channel widths, speed ratios, and transverse spacing to analyze their effects on the hydrodynamic interactions of the two-ship rendezvous. Ok et al. [28] utilized OpenFOAM for the single-ship and two-ship motions and compared the results of other software simulations and model tests to verify the effectiveness of CFD simulations. Wang et al. [29] simulated the process of two-ship meeting and catching up, analysed the effect of the attitude change of the ship on the inter-ship hydrodynamic force, and explored the effect of the ship speed ratio, transverse spacing, and scale ratio on the inter-ship hydrodynamic interactions. Zhou et al.[30] used the RANS-based CFD method to investigate the effect of the water depth, the relative speed, and the distance for the passing ship on the dock mooring The effect of water depth, relative speed and distance on passing ships on dock moorings was investigated, and it was found that the hydrodynamic force and moment change law of the moored ship in the case of relatively high speed was obviously different from that of low speed. Feng et al. [31] simulated the motion process of USV rapidly approaching the mother ship by using numerical wave pool technology, analyzed the motion response of the USV under different motion directions, and found that the USV is prone to capsize phenomenon when its motion direction is not in the center of the wake flow of the large ship. Yu et al. [32] used STAR-CCM+ to simulate the motion of two vehicles in regular waves in 2022, compared the motion response and force under different wavelengths and different transverse spacings, and analyzed the relationship between the ratio of wavelength, transverse spacing to the length of the vehicle, and the change of force.

Existing research work is less focused on the USV recovery process, especially on the interaction with the mother ship when the USV runs to different positions during the recovery process. The motion responses and forces of the USV are very complicated during the USV recovery process. In order to study the hydrodynamic characteristics of the USV during the recovery process, this paper uses the CFD method to

simulate the process of the USV chasing the mother ship. Firstly, the validity of the numerical simulations is verified. The simulations of the 175-USV chasing the KCS model scale model, the mother ship is carried out, with changing the chasing speed, wave amplitude and direction relative to the mother ship. The time varying motion responses and hydrodynamic forces of the USV, the wave and wake induced by the advancing mother ship are observed, compared and analysed in different cases.

## 2. Problem description

In this paper, the mother ship recovery process of USV mainly focuses on the process of the USV chasing the mother ship. The mother ship is running ahead while the USV is chasing behind till docking with the mother ship to finish the purpose of human rescues. They are shown schematically in Figure 2, with a 175-USV in Figure 3(a) and a mother ship that can be approximated as a KRISO Container Ship (KCS) in Figure 3(b). The USV is 175-USV made by Huazhong University of Science and Technology, with a length of 1.75 m developed and its specific parameters are shown in Table 1. The specific parameters are shown in Table 1.

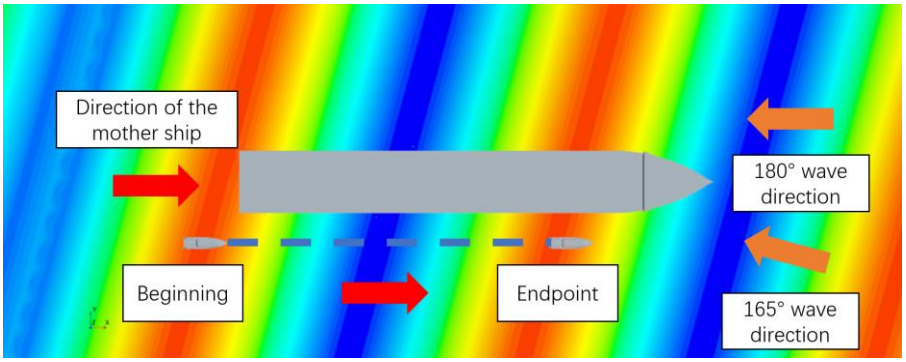


**Fig. 2** Scenario for USV chasing mother ship in waves

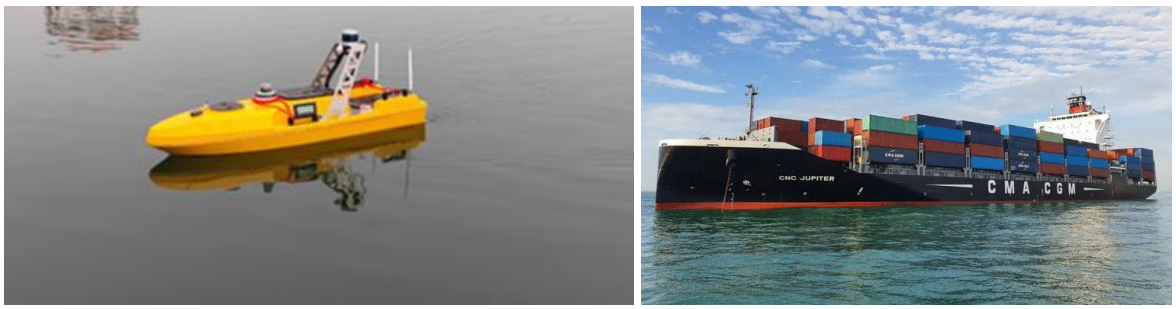


(a) 175-USV (b) KCS model ship [29]

**Fig. 3** USV and mother ship

**Table 1** Scale parameters related to USV and mother ship

| Parameter | Value |
|---|---|
| Length of the mother ship, m | 20 |
| Beam of the mother ship, m | 2.8 |
| Moulded depth of the mother ship, m | 1.65 |
| Displacement of the mother ship, kg | 940 |
| Length of the USV, m | 1.75 |
| Beam of the USV, m | 0.62 |
| Moulded depth of the USV, m | 0.25 |
| Displacement of the USV | 60 |

## 3. Numerical modelling

Computational domain is a virtual sea area that simulates the actual physical sea area by solving the fluid control equations in a numerical, discrete manner. There are two main theories established for the numerical sea domain: a boundary element method based on potential flow and an NS equation method based on viscous flow. The boundary element method is an indirect method, i.e., the ideal fluid forces are solved first, and the viscous forces are estimated by empirical equations; whereas the NS method based on viscous flow directly solves the forces acting on the navigational body, which includes the forces of the ideal fluid, and the method is more direct and accurate. In this paper, the NS equations will be used as the basis for a discrete solution using the finite volume method to establish a numerical virtual sea area, including numerical free sea area and towed sea area, to evaluate the motion characteristics of the USV in the environment of complex waves and mother ship interference.

### 3.1 Governing equation

The governing equations for a three-dimensional, non-stationary, Newtonian fluid are:

$$\frac{\partial(u_i)}{\partial x_i} = 0 \tag{1}$$

$$\frac{\partial(u_i)}{\partial t} + (u_j)\frac{\partial(u_i)}{\partial x_j} = -\frac{1}{\rho}\frac{\partial(p)}{\partial x_i} + v\frac{\partial^2(u_i)}{\partial x_j \partial x_j} - \frac{\partial(u_i' u_j')}{\partial x_j} + f_i \tag{2}$$

where Equation (1) is the continuity equation and Equation (2) is the Reynolds Averaged Navier-Stokes (RANS) equation. $u_i$ is the time-averaged value of the fluid velocity component, $t$ is the time, $v$ is the fluid kinematic viscosity coefficient, $\rho$ is the air-water density in the middle of the two-phase fluid domain, $u_i' u_j'$ is the Reynolds stress tensor, and $f_i$ is the volumetric force source term component.

### 3.2 Turbulence model

For the Reynolds averaging assumption, the turbulence models that close the RANS equations include the standard k-epsilon model in the two-equation model, the RNG k-epsilon model, Realizable k-epsilon model, which is developed based on it, and the other dominant two-equation model is the standard k-omega model, and the SST (Shear Stress Transport) k-omega model. Among them, the SST k-omega model is the most widely used one in engineering, which has high accuracy for both attached boundary layer turbulence and moderate separation turbulence, and is suitable for numerical calculation of ship maneuverability. In this project, the RANS method with the SST k-omega model is used as the controlling equation. The Reynolds stress tensor is expressed in the form suggested by Boussinesq using the classical vortex viscosity assumption [33]:

$$-\rho\overline{u_j u_i'} = \mu_t\left(\frac{\partial\overline{u_i}}{\partial x_j} + \frac{\partial\overline{u_j}}{\partial x_i}\right) - \frac{2}{3}\rho k\delta_{i,j} \tag{3}$$

where $k$ is the kinetic energy of turbulent pulsation per unit mass of fluid; $\mu_t$ is called turbulent eddy viscosity; $\delta_{i,j}$ is the Kronecker function. Using two two-equation model SST $k$-$\omega$ Turbulence model closed RANS equations, the model of the attached boundary layer turbulence and moderate separation of turbulence has high computational accuracy, about $k$ and unit dissipation rate $\omega$ of the equations are:

$$\frac{\partial}{\partial t}(\rho k) + \frac{\partial}{\partial x_i}(\rho k u_i) = \frac{\partial}{\partial x_j}\left(\Gamma_k \frac{\partial k}{\partial x_j}\right) + \widetilde{G_k} - Y_k + S_k \tag{4}$$

$$\frac{\partial}{\partial t}(\rho\omega)+\frac{\partial}{\partial x_i}(\rho\omega u_i)=\frac{\partial}{\partial x_j}\left(\Gamma_\omega\frac{\partial\omega}{\partial x_j}\right)+G_\omega-Y_\omega+D_\omega+S_\omega \tag{5}$$

Turbulent eddy viscosity $\mu_t$ is expressed as:

$$\mu_t=\rho\alpha^*\frac{k}{\omega} \tag{6}$$

where $\Gamma_k$ and $\Gamma_\omega$ are the effective diffusion terms for $k$ and $\omega$, respectively; $Y_k$ and $Y_\omega$ are the turbulent kinetic energy dissipation terms for $k$ and $\omega$, respectively; $D_\omega$ are the cross-diffusion terms; $S_k$ and $S_\omega$ are the customized source terms for k and $\omega$, respectively; and $\alpha^*$ are the model coefficients.

### 3.3 Volume of fluid method

In this paper, the Volume of Fluid (VOF) method is used to capture the variation of the free surface. The basic idea is to represent the fluid volume change in the mesh by the fluid volume function and construct the free water surface with its help, which is suitable for the solution of multiple incompatible fluid interfaces. The fluid volume function needs to satisfy the following equation [34, 35]:

$$\frac{\partial\alpha}{\partial \mathrm{t}}+u_i\frac{\partial\alpha}{\partial\xi}+u_j\frac{\partial\alpha}{\partial\eta}+u_k\frac{\partial\alpha}{\partial\zeta}=0 \tag{7}$$

where $u_i, u_j, u_k$ is the partial velocity of the fluid and $\alpha$ is the volume fraction of each cell. When $\alpha$ =1 it is exclusively water, when $\alpha$=0, it is exclusively air.

### 3.4 Wave-making and wave elimination methods

Currently, the common wave-making methods are the push plate wave-making method, the boundary wave-making method and the source term wave-making method. Compared with the other two methods, the boundary wave-making method directly amplitude of the wave's analytical solution at the boundary of the wave pool, can simulate both linear and nonlinear waves, and improves the efficiency and saves time [33, 34], so this paper adopts the boundary wave-making method. The wave dissipation method adopted in this paper is the boundary damping method, which adds the damping term in the vertical direction of the wave motion water quality point, so that the wave amplitude is gradually reduced. Compared with Sommerfeld's linear radiation condition method, which is used to solve linear problems, the boundary damping method is also suitable for nonlinear or irregular waves.

## 4. Numerical simulations of USV chasing mothership

The simulation scene is shown in Figure 4, and the specific flow of the simulation is as follows: the USV is moved from the aft part of the mother ship to move along the x-axis with the mother ship at a certain relative speed, and the wave can be loaded from the entrance. When the USV runs along the mother ship's length from the stern till passing the location of the docking cage, the simulation stops and the relevant motion response and force on the USV are recorded.

### 4.1 Computational domain and boundary conditions

The surfaces of the USV and the mother ship are no-slip walls. The geometric models of the mother ship and USV are shown in Figures 4 and 5. The computational domain is a large rectangular box-shaped sea area, as shown in Figure 6. The lateral face the setup USV moves towards is treated as the velocity inlet boundary, and the other lateral surface corresponds to the pressure outlet behind the USV. The remaining four faces of the square are all velocity inlets. The mother ship is a standard model with a length of 20 m, the USV was modelled with a length of 1.75 m, and the main parameters were consistent with those of the 175-USV described previously. In order to ensure that the forces and responses on the USV generated by the mother ship's rising waves and induced wakes are not affected by the boundary of the numerical sea area, the velocity

inlet in front of the mother ship is 0.5 times the length of the mother ship's bow, the pressure outlet is 1.5 times the length of the mother ship's stern, the left and right velocity inlets are 1 times the length of the mother ship's mid-longitudinal profile, and the upper and lower velocity inlets are 0.5 times the length of the mother ship's mid-transverse profile.

**Fig. 4** Geometric model of mother ship

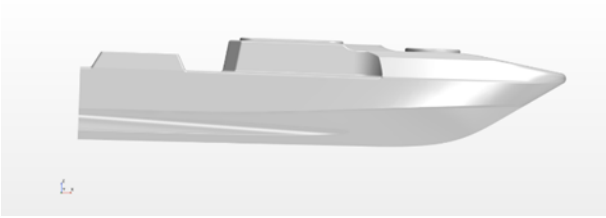

**Fig. 5** Geometric model of USV

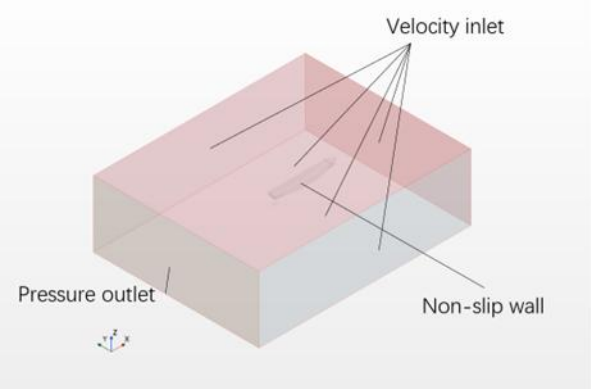


**Fig. 6** Computational domain and boundary conditions

## 4.2 Mesh arrangement

As shown in Figure 7, the mesh consists of a background mesh (large rectangle) and overlapping mesh (USV, mother ship), where the overlapping mesh is nested within the background mesh. The surface meshes of the mother ship and USV are refined to create accurate and undistorted wall boundaries. The motion capturing areas of the USV and mother ship are refined to improve the resolution and ensure computational accuracy, and the free water surface area is also refined. The wave simulation requires that grid sizes in the wave height and wavelength directions are not larger than one-twentieth of the wave height and one-hundredth of the wavelength in the wave height and wavelength direction. The grids are all structured grids, and the total number of grids varies from 9 million to 23 million depending on the working conditions.

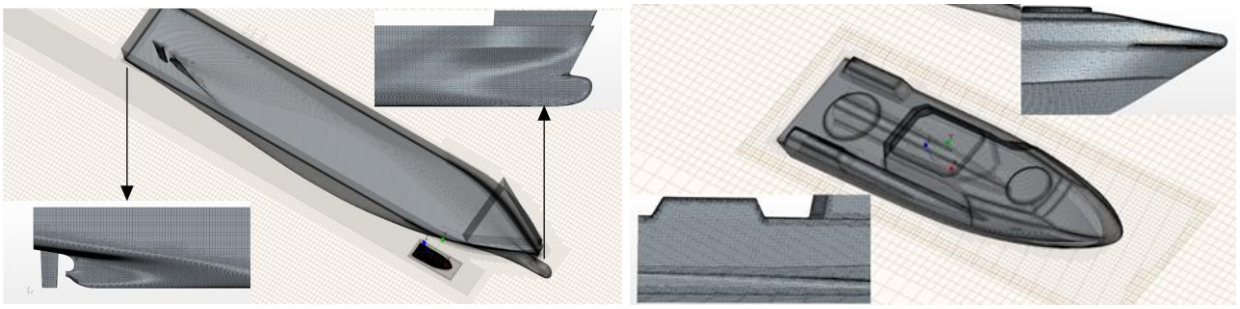

(a) Mother ship (b) USV

**Fig. 7** Mesh representations for USV and mother ship

## 4.3 Boundary layer treatment

The SST k-omega turbulence model is selected for this simulation, and the wall surface is treated in full $y^+$ wall treatment mode, using a hybrid wall function to treat the low Reynolds number region of the wall

attachment. Therefore, as shown in Figures 8 and 9, the wall boundary layer ensures that the $y^+$ of the wet surface area of the mother ship and most of the USV is around 25-150 to meet the accuracy requirements.

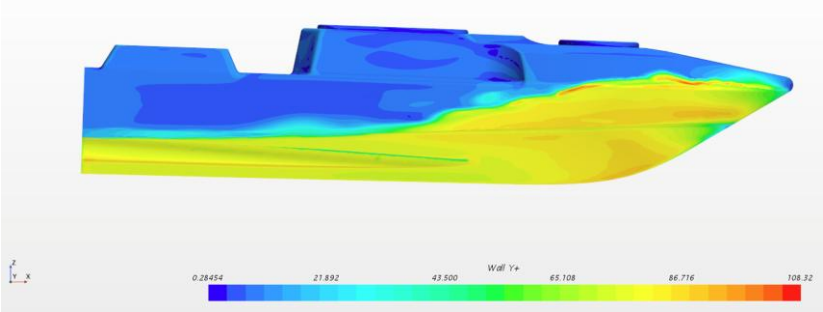


**Fig. 8** $y^+$ value on the surface of the USV

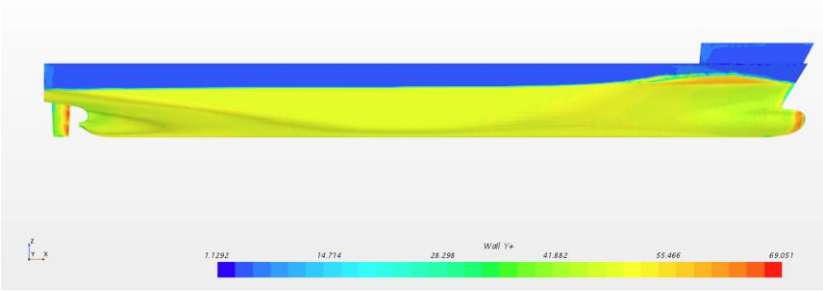


**Fig. 9** $y^+$ value on the surface of the USV

## 5. Experiment and validation study

In order to verify the validity of the simulation, the mother ship, a KCS standard model ($L$=6.07 m), is simulated and compared with the experimental data. The distribution of wave height along the mother ship's length in the calm water environment is verified at the running of $Fr$=0.26. The comparative results about wave elevations along the ship are shown in Figure 10. The simulated frictional, pressure and total resistance have only -1.8 %, 3.6 %, and -0.8 % difference from the calm water resistance experiment as shown in Table 2. The longitudinal and vertical oscillations in the calm water environment at the working condition of $Fr$=0.28 were also observed and obtained. Correspondingly, the comparison of numerical and experimental results as shown in Table 3 indicates that for $Fr$=0.28, the percentage difference of total resistance, heave and pitch motions between simulated and experimental results in calm water are 1.21 %, 2.88 %and -3.29 %, respectively. When recalling to check the KCS performance during its running at $Fr$=0.28 in wave environment, it is found that the simulated discrepancy is 6.25 % for the drag coefficient, and 0.0361 % and -5.58 % for the amplitude of heave and pitch motions are respectively. The results mentioned above indicate that the simulation approach used in this paper is not only suitable for mother ship advancing in calm water environment but also for the wave environment, as shown in Table 4.

**Table 2** Resistance Comparisons of KCS Standard Model at $Fr$=0.26

| - | Frictional resistance, N | Pressure resistance, N | Total resistance, N |
|---|---|---|---|
| Experiment | 64.2 | 16.4 | 80.7 |
| Simulation | 63 | 17 | 80 |
| Relative difference, % | -1.8 | 3.6 | -0.8 |

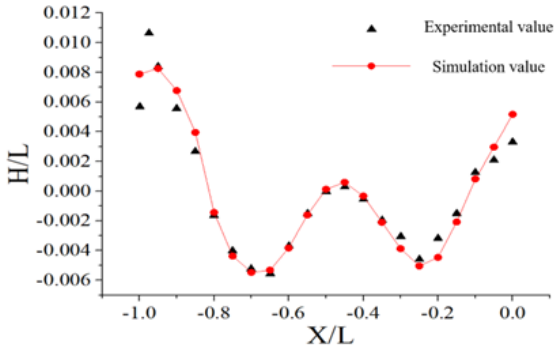


**Fig. 10** The distribution of relative wave elevations along the relative length of KCS standard model at the design speed (*Fr*=0.26)

**Table 3** Comparison of motion responses of KCS in calm water (*Fr*=0.28)

| - | Experiment | Simulation | Relative difference, % |
|---|---|---|---|
| Total resistance force, N | 120.5 | 122.0 | 1.21 |
| Heave, m | -0.01702 | -0.01751 | 2.88 |
| Pitch, rad | -0.1590 | -0.1538 | -3.29 |

**Table 4** Comparison of motion responses of KCS in wave environment (*Fr*=0.26)

| - | Mean value of drag coefficient, N | Heave, mm | Pitch |
|---|---|---|---|
| Experiment | 7.078E-03 | 55.4 | 2.38 |
| Simulation | 7.52E-03 | 55.42 | 2.247 |
| Relative difference, % | 6.25 | 0.0361 | -5.58 |

For checking and validating the simulated USV hydrodynamic performance of during its recovery, the self-propelled wave-making characteristics of the real USV, as shown in Figure 11, 175-USV made by Huazhong University of Science and Technology (HUST) are compared with the simulation results. The 175-USV and the relevant main parameters are shown in Table 5. In the lake test, 175-USV chases a small tugboat ahead with self-propelled speed of 2.24 m/s and 3.24 m/s, respectively. It is found that the simulated wave contour and the spreading angle at the bow and the stern of 175-USV are basically similar to those observed in this real USV recovery lake test as shown in Figure 11. In the USV lake test, the spreading angle was approximately 45° at $v$ = 2.24 m/s and 30° when $v$ = 2.34 m/s. The CFD simulation results showed much the same trend, with the spreading angle slightly greater than the experimental value at the same speed.

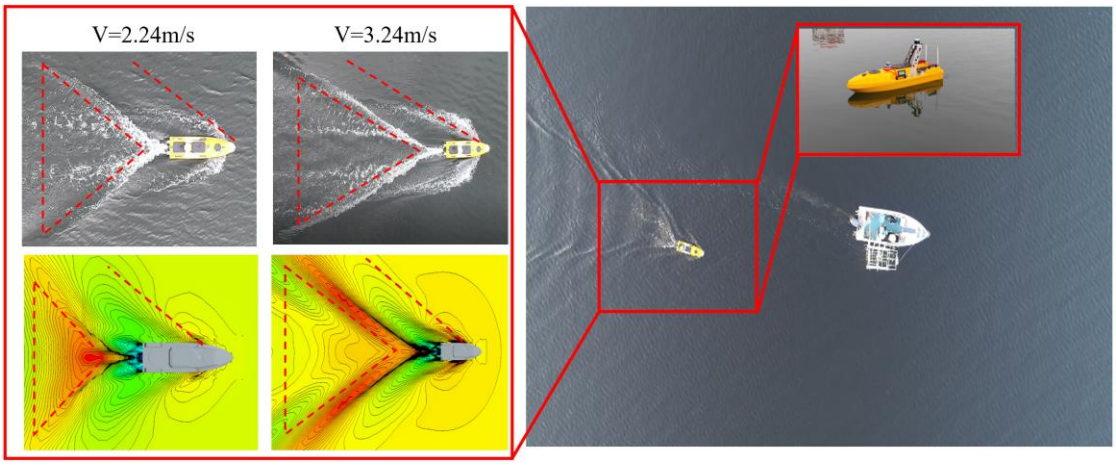


**Fig. 11** Comparison of simulated USV wave making characteristics to lake tests

**Table 5** Main parameter of 175-USV

| Target | Length, m | Beam, m | Depth, m | Max speed, kn | Duration, hr |
|---|---|---|---|---|---|
| 175-USV | 1.75 | 0.62 | 0.75 | 7 | 6 |

## 6. Case study and analysis

The USV is located far behind the mother ship at the initial moment. The USV and the mother ship are traveling forward at different speeds. The simulation is terminated when the USV passes the docking cage located at the starboard side of the mother ship. The motion response and force of the USV in this process are recorded and analysed. Specific simulation conditions are shown in Table 6 to investigate the effects of relative speed, wave height and wave direction on the motion and acting force of the USV, wave and wake induced by the mother ship. Among them, considering the differences in scale between the simulation model and the actual ship, the parameters used in the simulation for sea level state III were also scaled down.

**Table 6** Typical simulation cases

| No. | Direction of the waves | Wave level | Speed of the mother ship, m/s | Speed of the USV, m/s | Wave height, m | Peak period, 1/s |
|---|---|---|---|---|---|---|
| 1 | - | Calm water | 1.23 | 1.54 | 0 | 0 |
| 2 | - | Calm water | 1.23 | 1.85 | 0 | 0 |
| 3 | 180 | Sea level state III | 1.23 | 1.54 | 0.24 | 2.988 |
| 4 | 165 | Sea level state III | 1.23 | 1.54 | 0.24 | 2.988 |
| 5 | 180 | Sea level state III | 1.23 | 1.85 | 0.24 | 2.988 |
| 6 | 165 | Sea level state III | 1.23 | 1.85 | 0.24 | 2.988 |

### 6.1 USV chasing mother ship in calm water

#### 6.1.1 Motion response of the USV

In the calm water environment, the speed of the mother ship is 1.23 m/s, and the speed of the USV relative to the mother ship is 0.62 m/s; the actual speed of the USV is 1.85 m/s. The motion response of the USV obtained from the simulation is shown in Figure 12(a)-(c). As can be seen from the figure, the amplitude of the roll angle of the USV jumps to a negative peak and then a positive peak at the very beginning of USV catching up mother ship. Afterwards, the roll motion of the USV keeps decreasing from a positive angle to a negative angle, but with a small amplitude secondary oscillation during the whole chasing process. It is interesting to find that the roll angle almost stays at zero with very small oscillation amplitude at 35-45 % of the mother ship length from the stern, which means to is suitable for USV to dock with the cage. The heave motion behaves nearly low low-frequency regular sinusoidal fluctuations except for the USV just entering at the 0-5 % of the mother ship length from the stern. The pitch angle fluctuates near zero with an amplitude of 0.8 m before reaching almost the middle of the mother ship. Later, a peak pitch response occurs at the location of 50 % of the length of the ship from the stern. This may be induced by the bow rising wave interference.

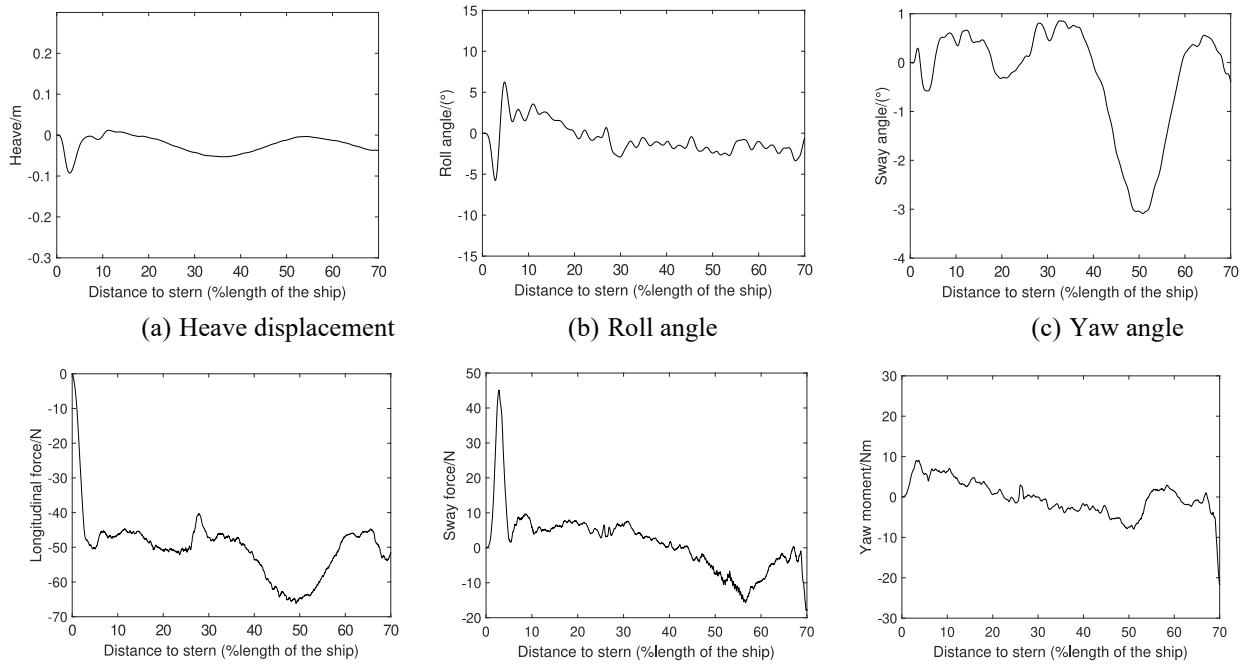


(a) Heave displacement (b) Roll angle (c) Yaw angle

(d) Surge force (e) Sway force (f) Yaw moment

**Fig. 12** USV dynamic responses chasing mother ship in calm water

### 6.1.2 Hydrodynamic forces acting on the USV

Sway and yaw motions are important factors which may influence the safety of USV by causing collisions with the mother ship because of lateral displacement and route change. Therefore, the sway force and yaw moment are observed and obtained as shown in Figure 12(d)-(f). The change of surge force corresponds to the change of resistance the USV will experience during the recovery process, while the yaw moment of the USV gives an explanation for the yaw angle changes observed in Figure 12(a)-(c). The change of the yaw moment from a positive peak to a negative peak causes the yaw angle oscillation near zero. When the yaw moment starts to jump to a positive peak, the yaw angle of the USV also starts to jump to a negative peak value. The oscillating sway force shows a decreasing trend as a whole, gradually changing from suction force (pulling the USV towards to mother ship) to repulsive force (pushing the USV away from the mother ship). The division point of the suction force turning to a repulsive force happens at about 40 % of the stern. Because of this cross-zero division, it is clear to see that the sway force at a range of 35-45 % from the stern is the smallest, which helps to explain why the roll angle stays at zero with very small oscillation amplitude at this range. When the USV arrives at the location 58 % from the stern, the repulsive decrease quickly. This may be because USV starts to encounter the bow-induced travelling waves and pushes the USV towards the mother ship as shown in Figure 12.

### 6.1.3 Wave-making status

In the calm water environment, the speed of the mother ship is 1.23 m/s, and the speed of the USV is 1.85 m/s relative to the mother ship, and the simulation of the wave made by mother ship is shown in Figure 13. It can be seen that when the USV is chasing from the stern to the bow on the side of the mother ship, the traveling wave generated by the mother ship itself such as spreading waves induced by bow and stern, wave troughs along the ship length especially at the center as shown in Figure 13 will interfere with the USV, as a result, the motion response and the acting force of the USV are also affected.

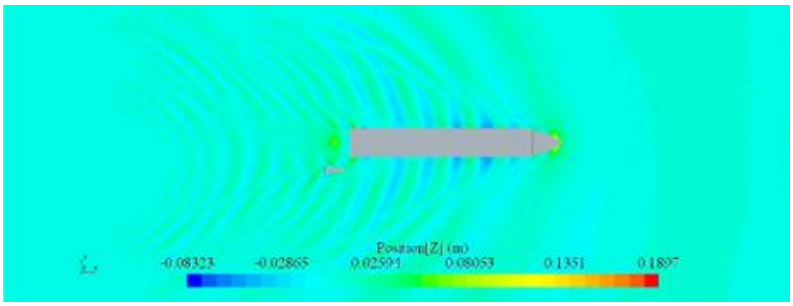


**Fig. 13** Wave making of the mother ship under calm water

## 6.2 USV chasing mother ship under wave condition

### 6.2.1 Motion responses of the USV

In the case of the mother ship's speed of 1.23 m/s, changing the wave direction (165°, 180°), the motion response of the USV obtained by simulation under different relative speeds of the USV (0.31 m/s, 0.62 m/s) is shown in Figure 14. In three-level (wave direction 165°, 180°) sea state, the heave and pitch of the USV are affected by the incoming wave and the traveling wave of the mother ship in a cyclic manner. The period of oscillation envelope is just the encountered period between the USV and the travelling wave of the mother ship, while the period of the high-frequency oscillations within the envelope is the encountered period between the USV and the incoming wave. The roll angle varies similarly to that in the calm water environment, maintaining a small oscillation at 35-45 % of the mother ship's length from the stern. With the sea state getting severe, the amplitude of the dynamic responses all increased as expected. The oblique waves excited larger motion responses than heading waves.

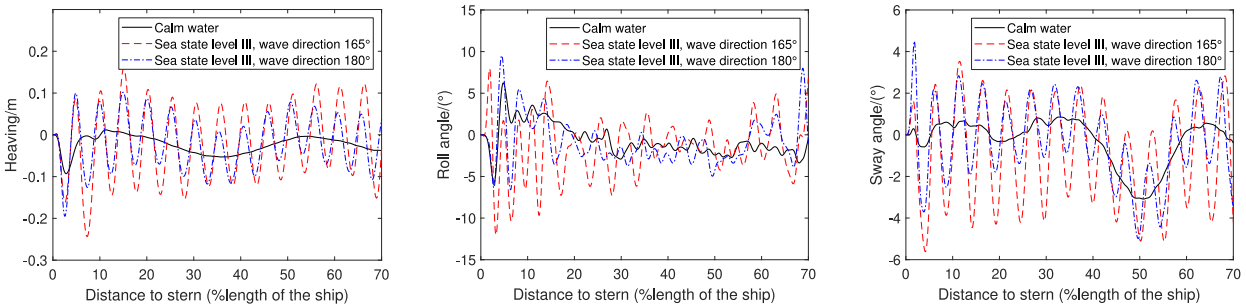


(a) Heave displacement (b) Roll angle (c) Pitch angle

**Fig. 14** The motion response of USV under different sea states for recovery

Correspondingly, the wave elevations around the USV, together with the motion responses of the USV at different moments in the 180° wave, are shown in Figure 15. When the USV is chasing from the stern to the bow of the mother ship, the USV gets gradually influenced by the bow scattering wave of the mother ship. From Figure 15, it can be seen that when the USV enters into the stern position of the mother ship, the USV's Roll angle and Heave displacement fluctuate greatly, and then tend to be stabilized with the continuation of its travel towards the bow. Subsequently, the Pitch angle fluctuates greatly during the 40-50 % stage.

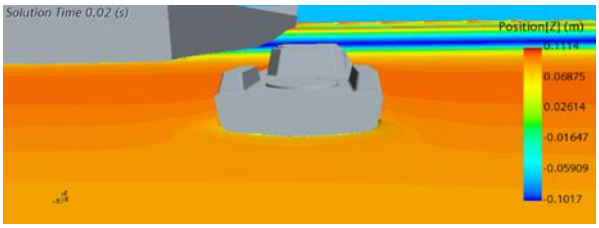


(a) Distance to stern 0 %

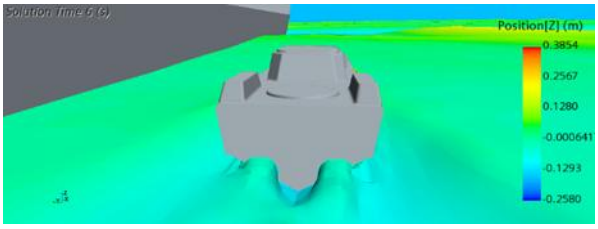


(b) Distance to stern 18.6 %

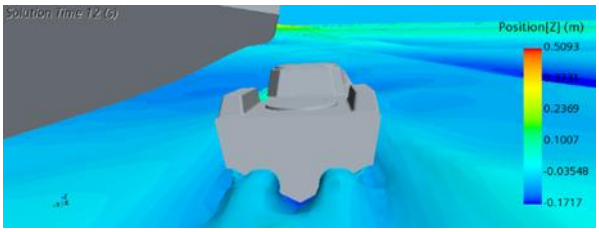


(c) Distance to stern 37.2 %

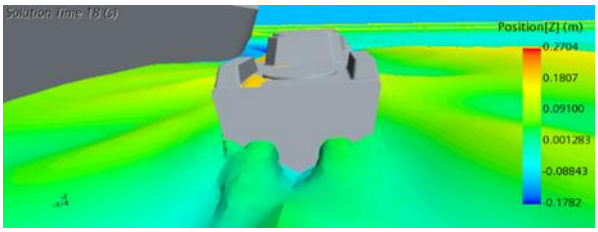


(d) Distance to stern 55.8 %

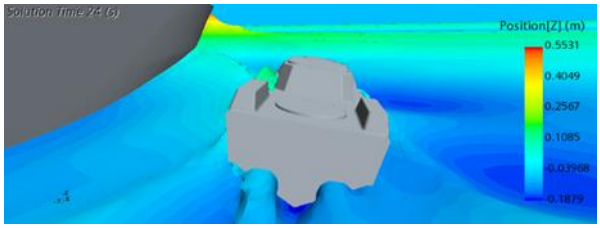


(e) Distance to stern 74 %

**Fig. 15** Wave making around USV at different distances to the stern of the mother ship under 180° wave direction

### 6.2.2 Hydrodynamic forces acting on the USV

The trend of USV force changes under wave conditions is similar to that in calm water. Also, the change of wave direction does not affect the characteristics and trends of the USV motion response and force. Also, the hydrodynamic forces such as surge, sway forces and yaw moment acting on USV are slightly larger than in calm water. However, the motion response and force amplitude of the USV are significantly larger under oblique waves compared to heading waves. At sea state class 3 with a wave direction of 165°, the surge forces increased significantly compared to the calm water condition, with the most pronounced increase occurring at 3-5 % of the distance to stern, when the USV first started sailing parallel to the mother ship, where the longitudinal forces increased by about 40 % compared to the calm water condition. The results of the sway force also show that the maximum force is found in the case of wave direction 165°, which is not only much larger than the case of calm water, but also 5-6 times larger than the case of wave direction 180°. The results are shown in Figure 16.

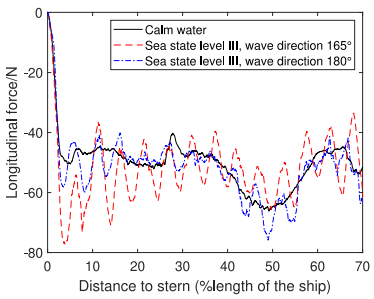


(a) Surge force time history

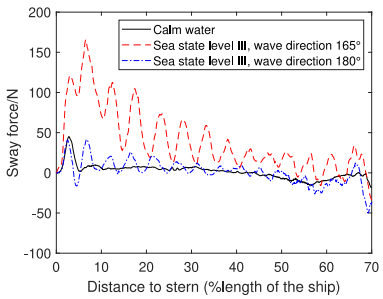


(b) Sway force time history

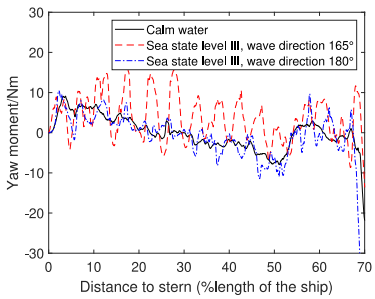


(c) Roll moment time history

**Fig. 16** Hydrodynamics forces acting on USV under different sea states

### 6.2.3 Wave-making analysis and USV chasing area planning

Under the sea state of level III (Wave period 7~8 s, wave height 1.25 m), the speed of the mother ship is 1.23 m/s, and the speed of the USV relative to the mother ship is 0.62 m/s, the simulations are obtained by changing the wave direction (165°, 180°). The simulated rising wave elevation contours for both directions are shown in Figure 17. It can be seen from the figure that the spreading angle of the USV is significantly lower in the wave direction of 165° compared to the working condition of 180° in the wave direction.

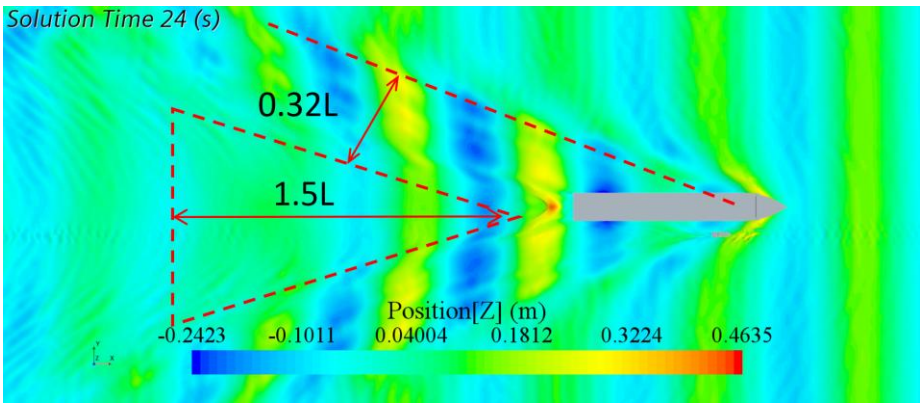


(a) 180° wave direction

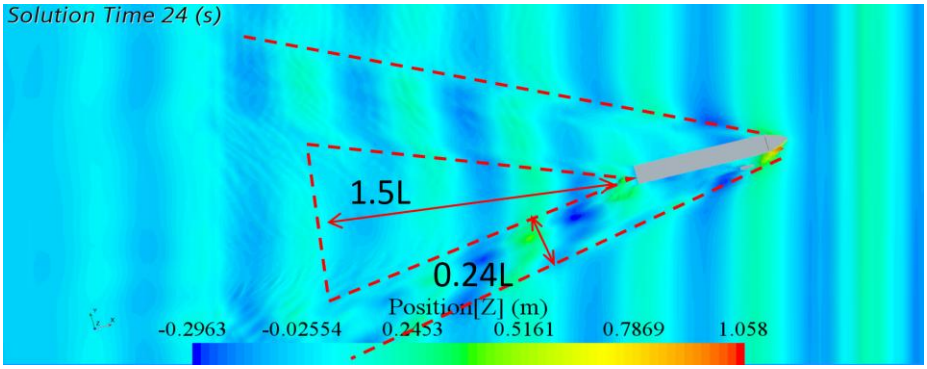


(b) 165° wave direction

**Fig. 17** Wave making of mother ship under Level 3 sea state and 165° and 180° wave direction

For heading waves, the wave height in the area between the bow scattering wave and the stern scattering wave is relatively small. So that means the wave dissipation is fast, which is favourable for the USV to chase and approach. For the oblique wave, the area between the bow scattering wave and the stern scattering wave on the side of the mother ship encountering the wave is further away from the mother ship than the heading wave condition. Also, the USV approaching the mother ship through this area has a larger entrance angle. Due to the blocking effect of the mother ship, there is a wave smooth zone on the other side of the mother ship encountering the wave, which is favourable for the recovery because of lower responses of the USV docking in the area.

## 7. Conclusion

This paper studies the hydrodynamic characteristics of an unmanned surface vehicle during the process of being recovered by a mother ship using a hoist system through computational fluid dynamics numerical simulation. The accuracy of the simulation is verified by the mother ship, KCS scale model, and lake surface tests tracking the 175-USV under the calm water and different incoming wave conditions. The changes in different relative velocities and wave directions are compared. During the chasing process, the lateral force of the USV changes from positive to negative, i.e., the suction force is applied from the stern to the bow and then gradually changes to the repulsion force. Also, it is found that when the unmanned surface vehicle is chasing in the range of 35-45 % of the mother ship's length from the stern of the mother ship, the roll angle oscillates

around zero, and the oscillating amplitude of roll angle and roll moment are very small, which is suitable for USV docking and recovery. In the wave environment, the USV is not only affected by the mother ship's rising wave, but also by the high-frequency perturbation of the incoming wave, so the addition of the waves makes the USV's response, and the amplitude of the force change more frequently, but the low frequency oscillation trend is similar to the calm water. Compared with the heading wave, the motion response and force amplitude of the USV increase significantly under the oblique wave, but meanwhile, the back side of the mother ship produces a wave smooth region to produce favourable conditions for recovery. The current research still has some limitations, including: a) numerical simulations did not consider the coupled effects of environmental factors such as wind and currents; b) experimental verification was only conducted for specific mother ship-USV size ratios and did not cover all scale conditions; c) wave directions were only selected at 165° and 180°, and the interference mechanisms at multiple angles were not systematically analyzed. Future work could focus on addressing these issues.

## ACKNOWLEDGMENTS

This work is supported by National Key R&D Program of China - Intergovernmental International Scientific and Technological Innovation and Cooperation Program (No. 2023YFE0115400), Hubei Provincial Natural Science Foundation (No. ZRMS2023001640), International Science and Technology Cooperation Project of Hubei Province (2024EHA030) and the National Natural Science Foundation of China (grant number 52571382). Also, this work contributes to the Strategic Research Plan of the Centre for Marine Technology and Ocean Engineering (CENTEC), which is financed by the Portuguese Foundation for Science and Technology (Fundação para a Ciência e Tecnologia - FCT) under contract UIDB/UIDP/00134/2020.

## REFERENCES

[1] Liu, C., Xiang, X., Huang, J., Yang, S., Zhang, S., Su, X., Zhang, Y., 2022. Development of USV autonomy: Architecture, implementation and sea trials. *Brodogradnja*, 73(1), 89-107. https://doi.org/10.21278/brod73105

[2] Xiang, G., Xiang, X., 2021. 3d trajectory optimization of the slender body freely falling through water using cuckoo search algorithm. *Ocean Engineering,* 235, 109354. https://doi.org/10.1016/j.oceaneng.2021.109354

[3] Yang, L., Xiang, X., Kong, D., Yang, S. 2024. Small modular AUV based on 3D printing technology: Design, implementation and experimental validation. *Brodogradnja*, 75(1), 75104. https://doi.org/10.21278/brod75104

[4] Li, B., Liang, H., Chen, X., Araujo, R., 2021. Study of telescopic gangway motions in time domain during offshore operation. *Ocean Engineering*, 230, 108692. https://doi.org/10.1016/j.oceaneng.2021.108692

[5] Li, J., Xiang, X., Dong, D., Yang, S. 2023. Prescribed time observer based trajectory tracking control of autonomous underwater vehicle with tracking error constraints. *Ocean Engineering*, 274, 114018. https://doi.org/10.1016/j.oceaneng.2023.114018

[6] Yuan, S., Liu, Z., Sun, Y., Wang, Z., Zheng, L., 2023. An event-triggered trajectory planning and tracking scheme for automatic berthing of unmanned surface vessel. *Ocean Engineering*, 273, 113964. https://doi.org/10.1016/j.oceaneng.2023.113964

[7] Zhang, Y., Han, Z., Zhou, X., Li, B., Zhang, L., Zhen, E., Wang, S., Zhao. Z., Guo, Z., 2023. METO-S2S: A S2S based vessel trajectory prediction method with Multiple-semantic Encoder and Type-Oriented Decoder. *Ocean Engineering*, 277, 114248. https://doi.org/10.1016/j.oceaneng.2023.114248

[8] Zhang, M., He, Y., Xiong, J., 2021. Research on the unmanned surface vehicle kinetics model for automatic berthing. In *Advances in Guidance, Navigation and Control: Proceedings of 2020 International Conference on Guidance, Navigation and Control*, ICGNC 2020, October 23–25, Tianjin, China, 3659-3670. https://doi.org/10.1007/978-981-15-8155-7_305

[9] Wu, G., Li, D., Ding, H., Shi, D., Han, B., 2024. An overview of developments and challenges for unmanned surface vehicle autonomous berthing. *Complex & Intelligent Systems*, 10(1), 981-1003. https://doi.org/10.1007/s40747-023-01196-z

[10] Sarda, E. I., Dhanak, M. R., 2016. A USV-based automated launch and recovery system for AUVs. *IEEE Journal of Oceanic Engineering*, 42(1), 37-55. https://doi.org/10.1109/JOE.2016.2554679

[11] Xiang, G., Xiang, X., Datla, R., 2023. Numerical study of a novel small waterplane area USV advancing in calm water and in waves using the higher-order Rankine source method. *Engineering Applications of Computational Fluid Mechanics*, 17, 2241892. https://doi.org/10.1080/19942060.2023.2241892

[12] Wang, Z., Xiang, X., Xiong, X., Yang, S., 2025. Position-based acoustic visual servo control for docking of autonomous underwater vehicle using deep reinforcement learning. *Robotics and Autonomous Systems*, 186, 104914. https://doi.org/10.1016/j.robot.2024.104914

[13] Gao, J., Zhang, Y., 2024. Ship collision avoidance decision-making research in coastal waters considering uncertainty of target ships. *Brodogradnja*, 75(2), 75203. https://doi.org/10.21278/brod75203

[14] Jian, W., Cao, D., Lo, E. Y., Huang, Z., Chen, X., Cheng, Z., Gu, H., Li, B., 2017. Wave runup on a surging vertical cylinder in regular waves. *Applied Ocean Research*, 63, 229-241. https://doi.org/10.1016/j.apor.2017.01.016

[15] An, G., Xiang, G., Xiang, X., Datla, R., 2023. Resistance prediction and optimization of tri-swach using hybrid surrogate model with particular consideration of outrigger layout. *Ocean Engineering*, 285, 115239. https://doi.org/10.1016/j.oceaneng.2023.115239

[16] Ohkusu, M., 1969. On the heaving motion of two circular cylinders on the surface of a fluid. *Reports of Research Institute for Applied Mechanics*, 17(58), 167-185. https://doi.org/10.5109/7170234

[17] Yeung, R.W., 1978. On the interactions of slender ships in shallow water. *Journal of Fluid Mechanics*, 85, 143-159. https://doi.org/10.1017/S0022112078000567

[18] Liu, X., Zou, Z., 2016. Numerical calculation of the hydrodynamic interaction between two ships meeting in restricted waterways. *Chinese Journal of Hydrodynamics*, 31, 151-160.

[19] Sutulo, S., Soares, C. G., Otzen, J. F., 2012. Validation of potential-flow estimation of interaction forces acting upon ship hulls in parallel motion. *Journal of Ship Research*, 56, 129-145. https://doi.org/10.5957/jsr.2012.56.3.129

[20] Nam, B., Park, J., 2018. Numerical simulation for a passing ship and a moored barge alongside quay. *International Journal of Naval Architecture and Ocean Engineering*, 10, 566-582. https://doi.org/10.1016/j.ijnaoe.2017.10.008

[21] Li, B., 2020. Multi-body hydrodynamic resonance and shielding effect of vessels parallel and nonparallel side-by-side. *Ocean Engineering*, 218, 108188. https://doi.org/10.1016/j.oceaneng.2020.108188

[22] Huang, J., Deng, Q., Xu, C., Zhuge, L., Ren, H., Zhou, X., 2021. Fast calculation method of ship-ship hydrodynamic interaction in restricted waters. *Journal of Harbin Engineering University*, 42, 601-609.

[23] Zheng, L., 2021. Analysis of the impact of docking methods on the hydrodynamic performance of ship. *Jiangsu Ship*, 38, 10–12. https://doi.org/10.19646/j.cnki.32-1230.2021.02.004

[24] Tafazzoli, S., Shafaghat, R., Alamian, R., 2021. Numerical investigation on the multi-body hydrodynamic interactions under caspian sea environmental conditions. *Ocean Engineering*, 232, 109048. https://doi.org/10.1016/j.oceaneng.2021.109048

[25] Ma, Z., Ji, N., Zeng, Q., Deng, X., Shi, C., 2024. Influence of scale effect on flow field offset for ships in confined waters. *Brodogradnja*, 75(1), 75106. https://doi.org/10.21278/brod75106

[26] Cong, P., Teng, B., Gou, Y., Tan, L., Liu, Y., 2022. Hydrodynamic analysis of resonant waves within the gap between a vessel and a vertical quay wall. *Ocean Engineering*, 260, 112192. https://doi.org/10.1016/j.oceaneng.2022.112192

[27] Zou, L., Larsson, L., 2013. Numerical predictions of ship-to-ship interaction in shallow water. *Ocean Engineering*, 72, 386-402. https://doi.org/10.1016/j.oceaneng.2013.06.015

[28] Ok, H., Lee, S., Choi, J., 2017. Numerical simulation of motion of single and side-by-side vessels in regular waves using openfoam. *Ships and Offshore Structures*, 12, 793-803. https://doi.org/10.1080/17445302.2016.1265697

[29] Wang, H. Z., Zou, Z. J., 2014. Numerical study on hydrodynamic interaction between a berthed ship and a ship passing through a lock. *Ocean Engineering*, 88, 409-425. https://doi.org/10.1016/j.oceaneng.2014.07.001

[30] Zhou, L., Abdelwahab, H., Soares, C. G., 2021. Experimental and CFD investigation of the effects of a high-speed passing ship on a moored container ship. *Ocean Engineering*, 228, 108914. https://doi.org/10.1016/j.oceaneng.2021.108914

[31] Feng, D. K., Jin, Z., Jun, Y., Yue, S., Xianzhou, W., 2020. Hydrodynamic analysis of the recovery of USV in regular waves. *China Journal of Ship Research*, 15, 38-44.

[32] Yu, X. Y., Wang, M. Q., Zhou, L. L., 2022. Numerical simulation of hydrodynamic interference between two vessels based on overlapped grids. *Ship Science and Technology*, 44, 6-11.

[33] Wang, H., Xiang, G., Yuan, Z., Xiang, X., 2023. Numerical study on hydrodynamic performance of ducted propeller based on improved body force model. *Chinese Journal of Ship Research*, 18.

[34] Yuan, Z. S., Xiang, G., Xiang, X. B., Huang, J. 2023. Numerical study on resistance of trimaran small waterplane area center hull under half constrained condition. *Shipbuilding of China*, 64, 192-204.

[35] Zhang, Q., Zhang, J., Chemori, A., Xiang, X., 2018. Virtual submerged floating operational system for robotic manipulation. *Complexity*, 2018(1), 9528313. https://doi.org/10.1155/2018/9528313